Chronic Perinatal Hypoxia Delays Cardiac Maturation in a Mouse Model for Cyanotic Congenital Heart Disease

Short Title: Romanowicz, Perinatal Hypoxia Delays Cardiac Maturation

Jennifer Romanowicz, MD[1], Zaenab Dhari, MD[2], Colm Mulvany, BS[3], Devon Guerrelli, MS[2,3], Marissa Reilly, BS[3], Luther Swift, PhD[3], Nimisha Vasandani, BS[2], Manelle Ramadan, BS[3], Nobuyuki Ishibashi, MD[1,2,3,4], Nikki Gillum Posnack, PhD[1,3,4]

[1]Children's National Heart Institute, Children's National Hospital, Washington, DC

[2]Center for Neuroscience Research, Children's National Hospital, Washington, DC

[3]Sheikh Zayed Institute for Pediatric Surgical Innovation, Children's National Hospital, Washington, DC

[4]Department of Pediatrics, Department of Pharmacology and Physiology, George Washington University, Washington DC

Corresponding author:

Nikki Gillum Posnack, Ph.D.

Sheikh Zayed Institute, 6th floor, M7707

111 Michigan Avenue, NW

Washington, DC, USA 20010

Tel: (202) 476-2475, Fax: (202) 476-2475

Email: nposnack@childrensnational.org

Subject Terms: Animal Models of Human Disease, Developmental Biology, Congenital Heart Disease, Electrophysiology, Contractile Function

Abstract

Background: Compared to acyanotic congenital heart disease (CHD), cyanotic CHD has an increased risk of lifelong mortality and morbidity. These adverse outcomes may be attributed to delayed cardiomyocyte maturation, since the transition from a hypoxic fetal milieu to oxygen rich postnatal environment is disrupted. To test the hypothesis that chronic perinatal hypoxia impairs cardiac maturation and functioning, we established a rodent model that replicates hypoxic myocardial conditions spanning perinatal cardiac development as observed in cyanotic CHD.

Methods: Mouse dams were housed in hypoxia beginning at embryonic day 16, coinciding with myocardial reliance on coronary flow. Pups stayed in hypoxia until postnatal day (P)8 when cardiac development is nearly complete. Global gene expression was quantified at P8 ($n \geq 4$) and at P30 after recovering in normoxia ($n \geq 4$). Phenotypic testing included electrocardiogram (P8 $n \geq 10$, P30 $n \geq 4$), echocardiogram (P30 $n \geq 3$), and *ex-vivo* electrophysiology study (P30 n=4).

Results: Hypoxic animals were 48% smaller than controls, consistent with intrauterine growth restriction observed in cyanotic neonates. Global gene expression was grossly altered by hypoxia at P8 (1427 genes affected), including changes in ion channels, sarcomere structure, and calcium handling. Gene expression changes normalized after recovery (P30). Electrocardiograms revealed bradycardia and slowed conduction velocity in hypoxic animals at P8, which resolved after recovery (P30). Notable differences that persisted after recovery (P30) included a 65% prolongation in ventricular effective refractory period, universal sinus node dysfunction, and a 24% reduction in contractile function in animals exposed to hypoxia.

Conclusions: This is the first study to investigate the impact of chronic hypoxia on the developing heart using both pre- and postnatal periods of hypoxia. Perinatal hypoxia was associated with changes in gene expression and cardiac functioning. Persistent changes to the

electrophysiologic substrate and contractile function warrant further investigation, and may contribute to adverse outcomes observed in the cyanotic CHD population.

Key Words: congenital heart disease, cardiac development, perinatal hypoxia, mouse, animal model cardiovascular disease

53 **Introduction**

54 Outcomes for patients with cyanotic congenital heart disease (CHD) remain guarded despite
55 countless advances in clinical care strategies over the last decades. CHD affects 1% of live
56 births[1], with one quarter of CHD representing cyanotic conditions[2]. Infants with cyanotic CHD
57 are at an 8-fold increased risk of death[2] compared to acyanotic CHD, and up to 39% of all
58 patients with CHD develop heart failure during childhood[3]. With clinical advances, the CHD
59 population is increasingly surviving to adulthood, leading to an increased burden of CHD-
60 associated heart failure[4]. Despite the high incidence of morbidity and mortality in the cyanotic
61 CHD population, the underlying risk factors are not fully understood[3].

62 Normal embryology of the heart directs streaming of the most highly saturated blood to the head
63 vessels and coronary arteries. For a fetus with complex CHD, this streaming pattern is disrupted
64 and the ascending aorta blood is desaturated[5]. Chronic hypoxic conditions in the developing
65 heart persist after birth until definitive repair. At the time of cardiac surgery, the cyanotic
66 myocardium has depleted endogenous antioxidants[6], higher tissue lactate levels[7], more
67 troponin I release[8], higher levels of oxidative stress[9], and less available adenosine triphosphate
68 (ATP)[10] compared to acyanotic myocardium. Moreover, cyanotic infants exhibit more myocardial
69 injury during bypass surgery and worse postoperative outcomes[8,10]. Little is known about the
70 mechanisms that contribute to the cyanotic myocardium's vulnerability to metabolic
71 derangements during surgery.

72 The transition from the hypoxic fetal milieu to the oxygen-rich postnatal environment is thought
73 to stimulate postnatal maturation[11]. Accordingly, a limited number of studies suggest that
74 hypoxia delays cardiac maturation. In mice, postnatal hypoxia prolongs the neonatal period of
75 cardiomyocyte proliferative ability[12]; and in chickens, prenatal hypoxia results in immature
76 calcium handling[13]. Moreover, cardiomyocytes sampled from human patients with hypoplastic
77 left heart syndrome show some persistence in fetal gene programming[14]. However, the direct

effects of chronic perinatal hypoxia on the developmental processes of the cardiomyocyte remain largely unknown.

To the best of our knowledge, this is the first study to examine the combined effects of pre- and postnatal hypoxia on the developing heart. The current study aimed to establish a rodent model of chronic perinatal hypoxia, as would be seen in cyanotic CHD, to investigate the developmental status of the cardiomyocyte under these conditions. We hypothesized that exposure to chronic hypoxia, beginning prenatally and continuing through the neonatal period, would perturb cardiomyocyte gene expression, contractile function, and the electrophysiologic substrate of the heart. The Cardiac Safety Research Consortium has implored the research community to perform more studies of developmental cardiac physiology to better understand the substrate on which therapies may work in the pediatric population[15], and this study intended to contribute to that call for knowledge.

Methods

Ethical Approval

Animal experiments were approved by the Institutional Animal Care and Use Committee at Children's National Research Institute, in compliance with the *NIH Guide for the Care and Use of Laboratory Animals*.

Animal Model

Wild-type pregnant CD1 mouse dams (6-8-week-old Crl:CD1(ICR) mice, Charles River Laboratories) were kept in a hypoxic chamber (BioSpherix, Redfield, NY) starting on embryonic day (E)16, a time that coincides with myocardial reliance on coronary flow for oxygen delivery and the beginning of a period of rapid growth of the ventricular myocardium, similar to the second trimester in human fetuses[16,17] (**Figure 1)**. During the experiment, the oxygen concentration was maintained, monitored, and recorded continuously with sensors placed inside

102 the chamber to achieve a level of 10.5 ± 0.5% (Pro:Ox Model 360, BioSpherix, Redfield, New
103 York). Nitrogen gas was used to displace oxygen. Dams gave birth in the hypoxic chamber and
104 pups remained in hypoxia until postnatal day (P)8, when cardiomyocyte maturation is nearly
105 complete[18,19]. Strain and age-matched normoxic dams were kept in normoxia and gave birth
106 under normoxic conditions. After P8, hypoxic animals were moved to normoxic conditions and
107 allowed to recover until further testing at P30, thus simulating the return to normal oxygen
108 saturations in human infants who have undergone definitive repair of cyanotic CHD.

109 *Gene Expression*

110 Whole hearts were excised and flash frozen in liquid nitrogen. Total RNA was isolated using an
111 RNeasy fibrous tissue kit. Verification of RNA integrity and RNA quantification were done by
112 spectrophotometry and an RNA 6000 Nano assay (Bioanalyzer 2100, Agilent Technologies).
113 The RNA integrity number for all samples was >6 (mean=8.6 +/- SEM 0.19). Total RNA (250 ng)
114 was primed for the entire length of RNA, including both poly(A) and non-poly(A) mRNA and
115 reverse transcribed to generate sense-strand targets that were biotin-labelled using a WT Plus
116 Reagent kit, and then hybridized to Affymetrix GeneChip Mouse Clariom S arrays for 16 hours
117 (48°C), following manufacturer's instructions (Thermo Fisher Scientific). Hybridization cocktails
118 were removed, and arrays were washed and stained on a Fluidics Station 450 (mouse Clariom
119 S arrays). Arrays were scanned on the Affymetrix GCS3000 7G scanner and initial quality
120 control data evaluated using Affymetrix Expression Console software (Thermo Fisher Scientific).
121 Microarray data was imported and analyzed using the Transcriptome Analysis Console (Applied
122 Biosciences). Gene ontology (GO) enrichment analysis was performed with the GOrilla tool
123 using a single rank-ordered gene list[20,21]. The GOrilla *Mus musculus* GO database is updated
124 frequently, and was last updated May 16, 2020 at the time of analysis.

125 *In-Vivo Electrocardiography*

126 Non-invasive electrocardiogram (ECG) recordings were obtained using an ecgTUNNEL system
127 (emka Technologies). ECG waveforms were recorded for two minutes on P8 conscious and
128 isoflurane-sedated animals as well as P30 conscious animals. ECG segments were quantified
129 using ecgAuto software (emka Technologies) for heart rate, heart rate variability, atrial
130 depolarization time (P-wave duration), atrioventricular conduction time (PR interval), ventricular
131 depolarization time (QRS duration), and ventricular repolarization time (QT interval). Heart rate
132 variability was measured as a root mean square of the successive differences (RMSSD)[22,23].

133 *Ex-Vivo Electrophysiology Study*

134 P30 animals were anesthetized with 4% isoflurane, the heart was rapidly excised and the aorta
135 cannulated. The heart was transferred to a temperature-controlled (37°C) constant-pressure (70
136 mmHg) Langendorff perfusion system. Excised hearts were perfused with Krebs-Henseleit
137 buffer bubbled with carbogen, as previously described[23,24]. A stimulation electrode was placed
138 externally on the right atrium, and an atrial pacing protocol was used to determine Wenckebach
139 cycle length (WBCL) and atrioventricular nodal effective refractory period (AVNERP). WBCL is
140 the shortest pacing cycle length during atrial pacing that causes the Wenckebach phenomenon.
141 AVNERP is the shortest extrastimulus interval during atrial pacing that fails to conduct through
142 the atrioventricular (AV) node, as indicated by loss of ventricular capture. For ventricular pacing,
143 a stimulation electrode was placed on the LV epicardium. To determine the ventricular effective
144 refractory period (VERP), dynamic pacing was performed with stepwise decrements in the
145 pacing cycle length (S1-S2) until loss of capture was noted. Baseline rhythms were monitored
146 throughout the duration of the studies for detection of dysrhythmias including ectopy, sinus node
147 dysfunction, and AV nodal block.

148 *High Frequency Ultrasound Echocardiography*

149 P30 animals underwent sedated transthoracic echocardiography to assess the persistent effects
150 of chronic perinatal hypoxia on left ventricular systolic function. Anesthesia was initiated and
151 maintained with inhaled isoflurane (1.5-2%). A pre-clinical high-frequency ultrasound system
152 (VisualSonics Vevo 770, 30mHz probe) was used to obtain fractional shortening in a parasternal
153 short axis view using M-mode measurements.

154 *Statistical Analysis*

155 Statistical analysis was performed using GraphPad Prism. Data normality was confirmed by
156 Shapiro-Wilk test. Datasets were compared using two-sample Student's independent t-test or 2-
157 way ANOVA with 0.1 false discovery rate to control for multiple comparisons testing (q value
158 reported). Nonparametric datasets were compared using the Mann-Whitney test. Significance
159 was defined as $p<0.05$.

160 **Results**

161 *Hypoxia decreased litter size and pup weight*

162 Hypoxic litters had markedly fewer pups than normoxic litters ($n\geq5$ litters per group, mean 5.7 vs
163 12.4 pups per litter, $p=0.0005$, **Figure 2A**). Intrauterine growth restriction is observed in human
164 newborns with cyanotic CHD[25,26]. Similarly, we observed that our hypoxic animals were smaller
165 than normoxic controls at P8 ($n\geq25$, mean 3.4 vs 6.5 g, $p<0.0001$, **Figure 2B-C**). Despite lower
166 body weight, heart weight was preserved in hypoxia such that it did not differ from control ($n=10$,
167 mean 46 vs 44 mg, $p=0.58$). As a result, heart-to-body-weight ratios were higher in hypoxic
168 animals ($n=10$, mean 8.0 vs 15.4 mg/g, $p<0.0001$).

169 After P8, hypoxic animals recovered in normoxic conditions, thus simulating the return to normal
170 oxygen saturations that occurs after definitive repair of cyanotic CHD. At P30, hypoxic animals
171 had undergone catch-up growth such that their body weight was only slightly lower than
172 normoxic controls ($n\geq14$, mean 20.0 vs 22.7 g, $p=0.015$, **Figure 2D**). Heart weight trended

173 toward slightly lower in hypoxic animals compared to control (n≥9, mean 119 vs 141 mg,
174 p=0.079), such that heart-to-body-weight ratios were equivalent between the groups (n≥9, mean
175 6.4 vs 6.3 mg/g, p=0.95).

176 *Hypoxia altered global gene expression at P8*

177 Gene expression arrays were performed on whole heart samples isolated at P8 to assess the
178 effects of hypoxia at the end of the neonatal period of rapid cardiomyocyte development, and
179 again at P30 after hypoxic animals had recovered in normoxia. Principal component analysis
180 demonstrated that experimental groups (normoxia versus hypoxia) were well-separated by their
181 mRNA expression profiles at P8, but this separation was negligible at P30 (**Figure 3A**). Using a
182 1.5-fold expression cut-off and a 10% false discovery rate to correct for multiple testing[27], a total
183 of 1427 mRNAs were differentially expressed between hypoxic and control hearts at P8 (**Figure**
184 **3B**; complete gene list in **Supplemental Table 1**). Differentially-expressed genes important to
185 cardiac functioning and development are highlighted in the **Figure 3C** volcano plot. Within
186 treatment groups, hypoxic animals exhibited a greater number of gene changes between P8
187 and P30 (4593 genes; **Figure 3B**) than the normoxic group (2147 genes), suggesting that the
188 hypoxic group underwent more developmental changes over this time period after transitioning
189 to normoxia. Interestingly, only one gene was expressed differentially between groups at P30:
190 Wsb2 (WD repeat and SOCS box-containing 2).

191 Differentially expressed genes at P8 were significantly overrepresented in >400 GO categories
192 (319 biological processes, 42 molecular functions, 46 cellular components**;** complete GO list in
193 **Supplemental Table 2**). Categories associated with phenotypic changes observed in our
194 experimental studies included extracellular matrix structural constituent (GO:0005201), ion
195 channel binding (GO:0044325), glycolytic process (GO:0006096), hypoxia-inducible factor-
196 1alpha signaling pathway (GO:0097411), mitotic cell cycle process (GO:1903047), and cell
197 maturation (GO:0048469) (**Figure 4**).

198 *Hypoxia altered transmembrane ion channel expression*

199 Multiple transmembrane ion channels were differentially expressed in P8 hypoxic animals,
200 including potassium (K^+), sodium (Na^+), and calcium (Ca^{++}) channels involved in the cardiac
201 action potential and maintenance of a stable resting membrane (**Figure 5A**). In ventricular
202 myocytes, phase 0 of the cardiac action potential is characterized by rapid depolarization via
203 Na^+ influx (I_{Na}); voltage-gated Na^+ channel gene expression was upregulated with hypoxia
204 (Scn3b: fold change +3.4, p=0.0002, q=0.017; Scn1b: fold change +1.3, p=0.018, q=0.15).
205 Phase 1 is characterized by a fast transient outward K^+ current (I_{to}), which was downregulated in
206 hypoxia (Kcnd2: fold change -8.02, p=0.0003, q=0.019; Kcnip2: fold change -3.17, p=0.0012,
207 q=0.042; Kcnd3: fold change -1.46, p=0.0079, q=0.10). Notably, decreased I_{to} current is also
208 observed in patients with atrial fibrillation[28] and heart failure[29], and can impair electromechanical
209 coupling and prolong action potential duration[30]. Phase 1 also includes slow Na^{++} efflux via the
210 Na^+/Ca^{++} exchanger (NCX1), which was upregulated in hypoxia (Slc8a1: fold change +2.78,
211 p=0.0001, q=0.012). The plateau phase (phase 2) is primarily responsible for action potential
212 duration. Membrane potential is held stable by balancing Ca^{++} influx and K^+ efflux, and both
213 were affected by hypoxia. Ca^{++} influx continues via NCX1 (upregulated in hypoxia, see above),
214 and L-type voltage-gated Ca^{++} channels open to increase Ca^{++} influx (I_{CaL}). I_{CaL} channels were
215 downregulated in hypoxia (Cacna2d1: fold change -1.96, p=0.0014, q=0.045). Calmodulin
216 expression was increased (Calm3: fold change +1.67, p=0.0009, q=0.036) which modulates
217 both action potential duration and excitation-contraction coupling by modifying I_{CaL}. Slow K^+
218 efflux (I_{Ks}) occurs via voltage-gated K^+ channels, which were upregulated in hypoxia (Kcnq1:
219 fold change +2.54, p=0.0057, q=0.089). Final rapid repolarization (phase 3) occurs mainly by K^+
220 efflux (I_{Kr}). Both genes associated with I_{Kr} trended toward downregulation (Kcne2: fold change -
221 1.47, p=0.22, q=0.51; Kcnh2: fold change -1.24, p=0.28, q=0.57). Finally, phase 4 represents

222 the resting membrane potential which is maintained via constant K^+ efflux (I_{K1}, I_{Ach}, I_{ATP}) through
223 inwardly rectifying K^+ channels; these genes were largely unaffected by hypoxia.

224 In cardiac pacemaker cells, the T-type Ca^{++} channel generates Ca^{++} influx (I_{CaT}) to initiate an
225 action potential (gene = Cacna1g). Cacna1g had a 3.13 fold down-regulation which did not meet
226 significance (p=0.052, q=0.26). Additional studies are needed to examine regional differences in
227 T-type Ca^{++} channel expression, which can result in bradycardia and sinus node dysfunction if
228 localized to pacemaker cells. Finally, gap junctions connect neighboring cardiomyocytes and
229 allow for rapid spread of an action potential from one cell to the next. Gap junction expression
230 was downregulated in hypoxia (Gja1: fold change -2.57, p=0.0022, q=0.056; Gja6: fold change -
231 1.74, p=0.0067, q=0.096), which can lead to slower electrical conduction.

232 *Hypoxia altered expression of genes important to the contractile apparatus*

233 Multiple genes important to the contractile apparatus were differentially expressed in P8 hypoxic
234 animals, including those involved in both calcium handling and sarcomere structure (**Figure**
235 **5B**). Within the cardiac sarcomere, isoform switching occurs during perinatal development for
236 many key structural proteins. In hypoxic P8 animals, there was persistence of immature
237 isoforms of Troponin-I (Tnni1: fold change +13.13, p=9.71E-05, q=0.011), alpha-actin (Acta1:
238 fold change +5.57, p=0.012, q=0.12), gamma-actin (Actg1: fold-change +3.05, p=0.010,
239 q=0.12), and myosin heavy chain (Myh7: fold change +1.48, p=0.083, q=0.32); although only
240 Troponin-I met the predetermined threshold for significance. The isoform switch for myosin light
241 chain was unaffected (Myl7→Myl2), however expression of two myosin light chain regulators
242 were altered (Myl3: fold change -1.79, p=0.0045, q=0.08; Myl9: fold change +5.48, p=0.0025,
243 q=0.06).

244 Multiple stabilizing components of the cardiac sarcomere were also altered in P8 hypoxic
245 animals. Titin, the cardiac myofilament responsible for passive tension, was downregulated in

246 hypoxia (fold change -2.56, p=0.0055, q=0.088), which may cause an increased risk for diastolic
247 dysfunction[31]. Desmin provides strength of attachment of myofibrils to the Z-disk, and was
248 upregulated in hypoxia (Des: fold change +2.31, p=0.0023, q=0.057). Desmosomes and
249 adherens junctions provide structural integrity between cells, and both demonstrated
250 downregulation of components in hypoxia (Pkp1: fold change -1.55, p=0.0022, q=0.056; Pcdh7:
251 fold change -1.82, p=0.0025, q=0.061; Dsc2: fold change -2.04, p=0.016, q=0.14). Vimentin
252 expression was increased (Vim: fold change +3.08, p=0.0017, q=0.050) indicating an increased
253 fibroblast population, but collagen expression was decreased (extracellular matrix cluster in
254 **Figure 4B**), suggesting decreased fibroblast functioning and a less robust extracellular matrix to
255 act as a scaffold for muscle contraction.

256 Calcium handling genes were also altered in hypoxic P8 animals. In mature cardiomyocytes,
257 synchronized ryanodine receptors facilitate a rapid increase in cytosolic Ca^{++} concentration
258 which is necessary for excitation-contraction coupling. Ryanodine receptor expression was
259 decreased in hypoxic animals (Ryr2: fold change -3.74, p=0.0038, q=0.073; Ryr1: fold change -
260 1.16, p=0.029, q=0.20), consistent with a delay in maturation. Further, extracellular Ca^{++} entry
261 may be altered in hypoxic animals due to decreased expression of L-type calcium channels
262 (Cacna2d1, see above) and increased expression of the Na^{+}/Ca^{++} exchanger (Slc8a1, see
263 above). The sarco-endoplasmic reticulum Ca^{++}-ATPase (SERCA) pumps calcium from the
264 cytoplasm back into the sarcoplasmic reticulum in preparation for the next cardiac cycle.
265 Hypoxia decreased SERCA expression (Atp2a3: fold change -2.03, p=0.0005, q=0.027), which
266 could decrease sarcoplasmic reticulum Ca^{++} load, reduce contractility, and slow lusitropy.

267 *Hypoxia caused bradycardia, slowed conduction velocity, and isoflurane effects at P8*

268 With the observed changes in ion channel expression on gene arrays, we collected *in-vivo* ECG
269 tracings at P8 (**Figure 6A**) to identify alterations in the electrophysiologic substrate of the heart
270 immediately after chronic perinatal hypoxia. During normal murine development, heart rate

271 increases as maturation progresses. At P8, hypoxic animals were bradycardic compared to
272 normoxic controls ($n \geq 10$, mean 308 vs 543 beats per minute, $p<0.0001$), consistent with a delay
273 in normal postnatal maturation (**Figure 6B**). We examined the effects of isoflurane sedation on
274 ECG measurements, as cyanotic newborns with CHD are subjected to anesthesia at the time of
275 surgical repair. Isoflurane sedation had a bradycardic effect in both groups; however, the
276 hypoxic animals remained more bradycardic than normoxic when sedated ($n \geq 10$, mean 204 vs
277 272 beats per minute, $q=0.0020$, **Figure 6C**).

278 Conduction speed is expected to increase throughout development as cell-cell interactions
279 mature. P8 hypoxic animals had a longer P-wave duration ($n \geq 7$, mean 15.0 vs 12.2 msec,
280 $p=0.017$), PR interval ($n \geq 8$, mean 53.0 vs 37.5 msec, $p<0.0001$), QRS duration ($n \geq 10$, mean
281 15.5 vs 13.3 msec, $p=0.012$), and QT interval ($n \geq 10$, mean 61.3 vs 38.8 msec, $p<0.0001$)
282 compared to normoxic controls (**Figure 6B**). QT intervals were analyzed in sedated animals, as
283 this parameter could not be measured accurately in active P8 animals. Isoflurane sedation
284 prolonged PR interval in both groups, but the effect was more dramatic in hypoxic animals ($n \geq 8$,
285 interaction $p=0.031$, $F=5.03$, **Figure 6C**). Anesthetic agents have been reported to slow
286 atrioventricular conduction in animal models[32,33] and human case reports[34,35], and our results
287 suggest that perinatal hypoxia exaggerates this effect. We also observed a significantly lower
288 heart rate variability in sedated hypoxic animals compared with normoxic controls ($n \geq 10$,
289 median 1.7 vs 3.4 msec, $q=0.0009$, **Figure 6C**). Importantly, heart rate variability increases with
290 age during normal development[23].

291 *ECG measurements normalized at P30 after a period of recovery in normoxia*

292 Since genetic differences had resolved at P30 after recovering in normoxia, ECG
293 measurements were repeated at P30 to determine if electrophysiologic differences had also
294 normalized. At P30, there was no difference in heart rate ($n \geq 4$, mean 407 vs 406 beats per
295 minute, $p=0.98$), heart rate variability ($n=4$, median 13.6 vs 8.0 msec, $q=0.34$), or QRS duration

296 (n≥4, mean 15.1 vs 15.3 msec, p=0.84) between groups (**Figure 6B**). Hypoxic animals still had
297 a trend toward longer P-wave duration (n≥4, mean 19.3 vs 16.1 msec, p=0.24), PR interval
298 (n≥4, mean 44.4 vs 38.9 milliseconds, p=0.39), and QT interval (n≥4, mean 23.9 vs 21.9 msec,
299 p=0.29) (**Figure 6B**). The significant differences in ECG parameters observed at P8 largely
300 abated after the 22 day period of recovery in normoxia, consistent with gene expression data
301 (**Figure 3A-B)**.

302 *Ex-vivo electrophysiology study revealed persistent underlying changes to the*
303 *electrophysiologic substrate after hypoxia*

304 Although ECG measurements largely normalized by P30, we conducted more rigorous testing
305 of the cardiac electrophysiologic substrate in the absence of autonomic influences.
306 Electrophysiology studies performed at P30 revealed that perinatal hypoxia caused persistent
307 prolongation of VERP compared to normoxic controls (n=4, mean 76.5 vs 46.5 msec, p=0.013),
308 a parameter that normally decreases with age (**Figure 7A**). No difference in atrioventricular
309 conduction was observed between groups, measured by WBCL (n=4, mean 84.0 vs 84.5 msec,
310 p=0.94) and AVNERP (n=4, mean 72.8 vs 70.5 msec, p=0.76) (**Figure 7A**). *Ex-vivo* studies also
311 revealed sinus node dysfunction in 100% of the hypoxic hearts, as opposed to 25% of the
312 normoxic control hearts (**Figure 7B,C**). Cyanotic CHD carries a high incidence of sinus node
313 dysfunction[36,37], and our results suggest that hypoxia may play a role in creating the substrate
314 for sinus node dysfunction.

315 *Perinatal hypoxia caused a persistent decrease in contractile function*

316 Gene expression changes indicated differences in the sarcomere and calcium handling at P8,
317 and we sought to measure phenotypic contractile function after recovery in normoxia.
318 Transthoracic echocardiography at P30 demonstrated decreased fractional shortening in

319 animals exposed to hypoxia as compared to normoxic controls ($n \geq 3$, mean 0.29 vs 0.38,
320 $p=0.027$, **Figure 8**), consistent with worse contractile function.

321 **Discussion**

322 Our results support our hypothesis that cardiac maturation is perturbed in a mouse model of
323 chronic perinatal hypoxia. Chronic perinatal hypoxia altered both the electrophysiologic
324 substrate and the contractile apparatus. Although the majority of differences detected at P8
325 normalized after recovering in normoxia, there were persistent alterations at P30 that may
326 contribute to lifelong mortality and morbidity in the cyanotic CHD population.

327 Numerous genetic and phenotypic differences were detected at P8. Hypoxia altered global gene
328 expression and ECG parameters, including bradycardia, slowed conduction speed, and
329 decreased heart rate variability and exaggerated PR prolongation with sedation. In our animal
330 model, P8 represents the time of surgical repair, and therefore, phenotypic differences in
331 hypoxic animals may have implications for surgical outcomes and the immediate post-surgical
332 course. Disturbances in ion channel expression may explain ECG disturbances at P8, and may
333 predispose the hypoxic heart to arrhythmias. Specifically, reduced I_{to} current and an altered
334 plateau phase can prolong the action potential, and reduced gap junctions can slow electrical
335 conduction across the heart. Likewise, decreases in extracellular matrix collagen and alterations
336 in the contractile apparatus have the potential to affect the strength of cardiac contraction.
337 Electromechanical coupling development was especially delayed in hypoxic animals, as
338 demonstrated by decreased L-type Ca^{++} channel, ryanodine receptor, and SERCA pump
339 expression; all of which can contribute to a blunted increase in cytosolic Ca^{++} concentration and
340 therefore weaker contraction. Increased dependence on glycolysis (**Figure 4**) may reduce
341 myocardial energy reserves, as observed in infants undergoing surgical repair[6–10]. Furthermore,
342 if myocardial growth continues by cell proliferation instead of hypertrophy, there is an increased
343 risk of cell structure abnormalities. Notably, some differentially expressed genes in our study are

344 associated with clinical sudden arrhythmic death syndromes[38] (long QT syndrome, Brugada
345 syndrome, arrhythmogenic right ventricular dysplasia, catecholaminergic polymorphic
346 ventricular tachycardia) and clinical cardiomyopathies[39] (dilated, hypertrophic, left ventricular
347 noncompaction).

348 In our model, P30 represents recovery after early definitive repair of cyanotic CHD. Gene
349 expression and ECG differences observed at P8 largely resolved by P30, suggesting that the
350 heart was able to complete development after a return to normal oxygen conditions. This is an
351 optimistic sign that many of the observed effects from chronic perinatal hypoxia may be
352 reversible with early repair. However, *ex-vivo* electrophysiology studies revealed persistent
353 changes to the underlying electrophysiologic substrate including prolonged VERP and
354 increased sinus node dysfunction, and echocardiogram revealed persistent decreased
355 contractile function. This is similar to previous animal studies of pre- or postnatal hypoxia, which
356 demonstrated both systolic and diastolic dysfunction[13,40–42]; however, this is the first study
357 demonstrating persistent electrophysiologic changes after perinatal hypoxia. Importantly,
358 measurements of gene expression do not necessarily reflect differences in protein expression
359 and localization, ion channel current, or the myofilament and sarcomere architecture. Studies
360 suggest that prenatal hypoxia imprints on a fetus and causes lifelong changes to the
361 cardiovascular system, such as increased susceptibility to systemic hypertension and metabolic
362 syndrome and worse response to myocardial infarction[43]. Further investigation is required to
363 define proteomic, metabolic, and ion current changes that persist after recovery from chronic
364 perinatal hypoxia.

365 To date, there has been limited investigation into the effects of hypoxia on the developing heart,
366 and thus there is no established animal model. The main embryological progression of heart
367 development is the same between humans and rodents[44]. The early embryonic heart is thin-
368 walled and relies on diffusion of oxygen from the chambers until the coronaries connect to the

369 aorta[44], at which point the myocardium starts to grow and thicken[18,44]. This timeline was the
370 rationale for starting hypoxia on embryonic day 16, when the coronary development is
371 complete[17,45]. This timing captures the period of rapid ventricular growth that occurs in both
372 species once the myocardium is reliant on the coronary circulation for oxygen delivery. For both
373 humans and rodents, there are similar changes in myocyte proteins for the remainder of
374 gestation, and both demonstrate rapid and marked development in the first postnatal week,
375 reaching definitive adult cell function and morphology quickly after the postnatal change in
376 loading conditions and oxygenation[18,19].

377 Our study aimed to be a proof of concept, that chronic perinatal hypoxia disrupts the process of
378 normal cardiac development. To our knowledge, this is the first study to include both pre- and
379 postnatal hypoxia to model the range of cardiac development affected by hypoxia in cyanotic
380 CHD. Further, we incorporated a period of recovery to simulate definitive repair of cyanotic
381 CHD. Toward this goal, our mice displayed characteristics consistent with human cyanosis,
382 such as lower birth weight[25,26], and replicated increased heart-to-body-weight ratios reported in
383 previous hypoxia animal studies[46,47]. Limitations of our model include the inherent constraints of
384 using small animals to model human disease, and the risk of introducing maternal stress into
385 gestation[48,49]. Litter size was reduced in our animals, which may be evidence for maternal
386 stress. Importantly, the comparative effect of degree of hypoxia between species is unknown.
387 We chose 10.5% for the degree of hypoxia, as a fractional inspired oxygen concentration (FiO_2)
388 of 10% correlates with pulse oximetry readings of 55-70% in rodents[50]. For comparison, human
389 fetuses with cyanotic CHD have a mean oxygen saturation of 48% in the ascending aorta[5], and
390 neonates have target oxygen saturation ranges of 70-85%. Despite the unknowns between
391 species, we believe this study is a first step toward understanding the impact of hypoxia on
392 cardiac development.

393 The Cardiac Safety Research Consortium has implored the research community to perform
394 more studies of developmental cardiac physiology to better understand the substrate on which
395 cardiac therapies may work in the pediatric population[15]. Further studies regarding the effects of
396 hypoxia on cardiac development may allow us to better target cardiac therapeutics for the
397 cyanotic CHD population. A better understanding of the effects of chronic perinatal hypoxia on
398 cardiac development could lead to improved surgical outcomes and overall improved
399 cardiovascular health in the cyanotic CHD population.

400 **Acknowledgments:** We gratefully acknowledge Dr. Susan Knoblach, Karuna Panchapakesan,
401 and the Children's National Research Institute Genomics and Bioinformatics Core for assistance
402 with microarray experiments; we also acknowledge Dr. Norman Lee for assistance with
403 heatmap analysis, and Drs. Christopher Spurney and Charles Berul for helpful discussions.

404 **Sources of Funding:** This work was supported by the NIH (R01HL139472 to NGP,
405 R01HL139712 and R01HL146670 to NI), Children's National Heart Institute, and the Office of
406 the Assistant Secretary of Defense for Health Affairs through the Peer Reviewed Medical
407 Research Program under Award No. W81XWH2010199 (N.I.). This publication was also
408 supported by the Gloria and Steven Seelig family.

409 **Disclosures:** None.

410 **Author Contributions:** JR, ZD, CM, DG, MR, LS, NV, MR performed experiments; JR, ZD,
411 CM, NGP analyzed data; JR, DG, NGP prepared figures; JR, NGP drafted manuscript; JR, ZD,
412 NI, NGP conceived and designed experiments; all authors approved manuscript.

413 **References**

414 1. Reller MD, Strickland MJ, Riehle-Colarusso T, Mahle WT, Correa A. Prevalence of
415 Congenital Heart Defects in Metropolitan Atlanta, 1998-2005. *J Pediatr*. 2008;153:807–
416 813.

417 2. Oster ME, Lee KA, Honein MA, Riehle-Colarusso T, Correa A. Temporal Trends in
418 Survival Among Infants With Critical Congenital Heart Defects HHS Public Access.
419 *Pediatrics*. 2013;131:1502–1508.

420 3. Hinton RB, Ware SM. Heart Failure in Pediatric Patients with Congenital Heart Disease.
421 *Circ Res*. 2017;120:978–994.

422 4. Dinardo JA. Heart failure associated with adult congenital heart disease. *Semin*
423 *Cardiothorac Vasc Anesth*. 2013;17:44–54.

424 5. Sun L, Macgowan CK, Sled JG, Yoo S-J, Manlhiot C, Porayette P, Grosse-Wortmann L,
425 Jaeggi E, McCrindle BW, Kingdom J, Hickey E, Miller S, Seed M. Reduced Fetal
426 Cerebral Oxygen Consumption is Associated With Smaller Brain Size in Fetuses With
427 Congenital Heart Disease. *Circulation*. 2015;131:1313–1323.

428 6. Teoh KH, Mickle DA, Weisel RD, Li RK, Tumiati LC, Coles JG, Williams WG. Effect of
429 oxygen tension and cardiovascular operations on the myocardial antioxidant enzyme
430 activities in patients with tetralogy of Fallot and aorta-coronary bypass. *J Thorac*
431 *Cardiovasc Surg*. 1992;104:159–64.

432 7. Modi P, Suleiman MS, Reeves BC, Pawade A, Parry AJ, Angelini GD, Caputo M. Basal
433 metabolic state of hearts of patients with congenital heart disease: The effects of
434 cyanosis, age, and pathology. *Ann Thorac Surg*. 2004;78:1710–1716.

435 8. Imura H, Caputo M, Parry A, Pawade A, Angelini G, Suleiman M. Age-Dependent and
436 Hypoxia-Related Differences in Myocardial Protection During Pediatric Open Heart
437 Surgery Improved Surgical Outcome After Fetal Diagnosis of Hypoplastic Left Heart
438 Syndrome. *Circulation*. 2001;103:1551–1556.

439 9. Ercan S, Cakmak A, Kösecik M, Erel O. The oxidative state of children with cyanotic and
440 acyanotic congenital heart disease. *Anadolu Kardiyol Derg*. 2009;9:486–90.

441 10. Najm HK, Wallen WJ, Belanger MP, Williams WG, Coles JG, Arsdell GS Van, Black MD,
442 Boutin C, Wittnich C. Does the degree of cyanosis affect myocardial adenosine
443 triphosphate levels and function in children undergoing surgical procedures for congenital
444 heart disease? *J Thorac Cardiovasc Surg*. 2000;119:515–524.

445 11. Patterson AJ, Zhang L. Hypoxia and fetal heart development. *Curr Mol Med*.
446 2010;10:653–66.

447 12. Puente BN, Kimura W, Muralidhar SA, Moon J, Amatruda JF, Phelps KL, Grinsfelder D,
448 Rothermel BA, Chen R, Garcia JA, Santos CX, Thet S, Mori E, Kinter MT, Rindler PM,
449 Zacchigna S, Mukherjee S, Chen DJ, Mahmoud AI, Giacca M, Rabinovitch PS,
450 Aroumougame A, Shah AM, Szweda LI, Sadek HA. The oxygen-rich postnatal
451 environment induces cardiomyocyte cell-cycle arrest through DNA damage response.
452 *Cell*. 2014;157:565–579.

453 13. Jonker SS, Giraud GD, Espinoza HM, Davis EN, Crossley DA. Effects of chronic hypoxia
454 on cardiac function measured by pressure-volume catheter in fetal chickens. *Am J*
455 *Physiol Integr Comp Physiol*. 2015;308:R680–R689.

456 14. Bohlmeyer TJ, Helmke S, Ge S, Lynch J, Brodsky G, Sederberg JH, Robertson AD,
457 Minobe W, Bristow MR, Perryman MB. Hypoplastic left heart syndrome myocytes are

458 differentiated but possess a unique phenotype. *Cardiovasc Pathol*. 2003;12:23–31.

459 15. Bates KE, Vetter VL, Li JS, Cummins S, Aguel F, Almond C, Dubin AM, Elia J, Finkle J,
460 Hausner EA, Joseph F, Karkowsky AM, Killeen M, Lemacks J, Mathis L, McMahon AW,
461 Pinnow E, Rodriguez I, Stockbridge NL, Stockwell M, Tassinari M, Krucoff MW,
462 Providence U. Pediatric cardiovascular safety: Challenges in drug and device
463 development and clinical application. *Am Heart J*. 2012;164:481–492.

464 16. Olivey HE, Compton LA, Barnett J V. Coronary Vessel Development The Epicardium
465 Delivers. *Trends Cardiovasc Med*. 2004;14:247–251.

466 17. Theveniau-Ruissy M, Perez-Pomares J-M, Parisot P, Baldini A, Miquerol L, Kelly RG.
467 Coronary stem development in wild-type and Tbx1 null mouse hearts. *Dev Dyn*.
468 2016;245:445–459.

469 18. Porter GA, Hom JR, Hoffman DL, Quintanilla RA, Bentley KL d. M, Sheu SS.
470 Bioenergetics, mitochondria, and cardiac myocyte differentiation. *Prog Pediatr Cardiol*.
471 2011;31:75–81.

472 19. Scuderi GJ, Butcher J. Naturally Engineered Maturation of Cardiomyocytes. *Front Cell*
473 *Dev Biol*. 2017;5:1–28.

474 20. Eden E, Navon R, Steinfeld I, Lipson D, Yakhini Z. GOrilla: A Tool For Discovery And
475 Visualization of Enriched GO Terms in Ranked Gene Lists. *BMC Bioinformatics*.
476 2009;10:48.

477 21. Eden E, Lipson D, Yogev S, Yakhini Z. Discovering Motifs in Ranked Lists of DNA
478 sequences. *PLoS Comput Biol*. 2007;3:e39.

479 22. Task Force of the European Society of Electrophysiology. Heart Rate Variability:

480 Standards of Measurement, Physiological Interpretation, and Clinical Use. *Circulation*.
481 1996;93:1043–1065.

482 23. Swift LM, Burke M, Guerrelli D, Reilly M, Ramadan M, McCullough D, Prudencio T,
483 Mulvany C, Chaluvadi A, Jaimes R, Posnack NG. Age-dependent changes in
484 electrophysiology and calcium handling: implications for pediatric cardiac research. *Am J*
485 *Physiol Circ Physiol*. 2020;318:H354–H365.

486 24. Jaimes R, McCullough D, Siegel B, Swift L, McInerney D, Hiebert J, Perez-Alday E,
487 Trenor B, Sheng J, Saiz J, Tereshchenko L, Posnack N. Plasticizer Interaction With the
488 Heart: Chemicals Used in Plastic Medical Devices Can Interfere With Cardiac
489 Electrophysiology. *Circ Arrhythm Electrophysiol*. 2019;12:e007294.

490 25. Malik S, Cleves MA, Zhao W, Correa A, Hobbs CA. Association Between Congenital
491 Heart Defects and Small for Gestational Age. *Pediatrics*. 2007;119:e976-982.

492 26. Khoury MJ, Erickson JD, Cordero F, Mccarthy BJ. Congenital Malformations and
493 Intrauterine G rowth Retardation : A Population Study. *Pediatrics*. 1988;82:83–90.

494 27. Posnack NG, Lee NH, Brown R, Sarvazyan N. Gene expression profiling of DEHP-
495 treated cardiomyocytes reveals potential causes of phthalate arrhythmogenicity.
496 *Toxicology*. 2011;279:54–64.

497 28. Brandt MC, Priebe L, Böhle T, Südkamp M, Beuckelmann DJ. The ultrarapid and the
498 transient outward K+ current in human atrial fibrillation. Their possible role in
499 postoperative atrial fibrillation. *J Mol Cell Cardiol*. 2000;32:1885–1896.

500 29. Beuckelmann DJ, Näbauer M, Erdmann E. Alterations of K+ currents in isolated human
501 ventricular myocytes from patients with terminal heart failure. *Circ Res*. 1993;73:379–385.

502 30. Niwa N, Nerbonne JM. Molecular determinants of cardiac transient outward potassium
503 current (Ito) expression and regulation. *J Mol Cell Cardiol*. 2010;48:12–25.

504 31. Lewinter MM, Granzier H. Cardiac Titin-A Multifunctional Giant. *Circulation*.
505 2010;121:2137–2145.

506 32. Kato K, Wakai J, Ozawa K, Sekiguchi M, Katahira K. Different sensitivity to the
507 suppressive effects of isoflurane anesthesia on cardiorespiratory function in SHR/Izm,
508 WKY/Izm, and Crl:CD (SD) rats. *Exp Anim*. 2016;65:393–402.

509 33. Raatikainen PMJ, Morey TE, Druzgala P, Milner P, Gonzalez MD, Dennis DM. Effects of
510 Volatile Anesthetics on Atrial and AV Nodal Electrophysiological Properties in Guinea Pig
511 Isolated Perfused Heart. *Anesthesiology*. 1998;89:434–442.

512 34. Mamiya K, Aono J, Manabe M. Complete atrioventricular block during anesthesia. *Can J*
513 *Anaesth*. 1999;46:265–267.

514 35. Kamatani T, Akizuki A, Kondo S, Shirota T. Second-Degree Atrioventricular Block
515 Occurring After Tooth Extraction. *Anesth Prog*. 2016;63:156–159.

516 36. Carlson SK, Patel AR, Chang PM. Bradyarrhythmias in Congenital Heart Disease.
517 doi:10.1016/j.ccep.2017.02.002.

518 37. Triedman JK. Arrhythmias in adults with congenital heart disease. *Heart*. 2002;87:383–
519 389.

520 38. Fulgent. Comprehensive Arrhythmia NGS Panel | Fulgent Genetics. Available at
521 https://www.fulgentgenetics.com/comprehensive-arrhythmia. Accessed May 14, 2020.

522 39. Fulgent. Comprehensive Cardiomyopathy NGS Panel | Fulgent Genetics. Available at
523 https://www.fulgentgenetics.com/comprehensive-cardiomyopathy. Accessed May 14,

524 2020.

525 40. Thompson LP, Chen L, Polster BM, Pinkas G, Song H. Prenatal hypoxia impairs cardiac
526 mitochondrial and ventricular function in guinea pig offspring in a sex-related manner. *Am*
527 *J Physiol Regul Integr Comp Physiol*. 2018;315:R1232–R1241.

528 41. Lindgren I, Altimiras J. Prenatal hypoxia programs changes in-adrenergic signaling and
529 postnatal cardiac contractile dysfunction. *Am J Physiol Regul Integr Comp Physiol*.
530 2013;305:1093–1101.

531 42. Corno AF, Giuseppina Milano F, Samaja M, Tozzi P, von Segesser LK. Chronic hypoxia:
532 A model for cyanotic congenital heart defects Corno et al Surgery for Congenital Heart
533 Disease. *J Thorac Cardiovasc Surg*. 2002;124:105.

534 43. Giussani DA, Davidge ST. Developmental programming of cardiovascular disease by
535 prenatal hypoxia. *J Dev Orig Health Dis*. 2013;4:328–337.

536 44. Wessels A, Sedmera D. Developmental anatomy of the heart: A tale of mice and man.
537 *Physiol Genomics*. 2003;15:165–176.

538 45. Savolainen SM, Foley JF, Elmore SA. Histology atlas of the developing mouse heart with
539 emphasis on E11.5 to E18.5. *Toxicol Pathol*. 2009;37:395–414.

540 46. Camm EJ, Hansell JA, Kane AD, Herrera EA, Lewis C, Wong S, Morrell NW, Giussani
541 DA. Partial contributions of developmental hypoxia and undernutrition to prenatal
542 alterations in somatic growth and cardiovascular structure and function. *Am J Obstet*
543 *Gynecol*. 2010;203:495.e24-495.e34.

544 47. Corno AF, Milano G, Samaja M, Tozzi P, von Segesser LK. Chronic hypoxia: A model for
545 cyanotic congenital heart defects. *J Thorac Cardiovasc Surg*. 2002;124:105–112.

546 48. Steurer MA, Peyvandi S, Baer RJ, Oltman SP, Chambers CD, Norton ME, Ryckman KK,
547 Moon-Grady AJ, Keller RL, Shiboski SC, Jelliffe-Pawlowski LL. Impaired Fetal
548 Environment and Gestational Age: What Is Driving Mortality in Neonates With Critical
549 Congenital Heart Disease? *J Am Heart Assoc*. 2019;8. doi:10.1161/JAHA.119.013194.

550 49. Gaynor JW, Parry S, Moldenhauer JS, Simmons RA, Rychik J, Ittenbach RF, Russell
551 WW, Zullo E, Ward JL, Nicolson SC, Spray TL, Johnson MP. The impact of the maternal-
552 foetal environment on outcomes of surgery for congenital heart disease in neonates. *Eur*
553 *J Cardiothorac Surg*. 2018;54:348–353.

554 50. Morgan BJ, Adrian R, Bates ML, Dopp JM, Dempsey JA. Quantifying hypoxia-induced
555 chemoreceptor sensitivity in the awake rodent. *J Appl Physiol*. 2014;117:816–824.

556 **Figures with Figure Legends:**

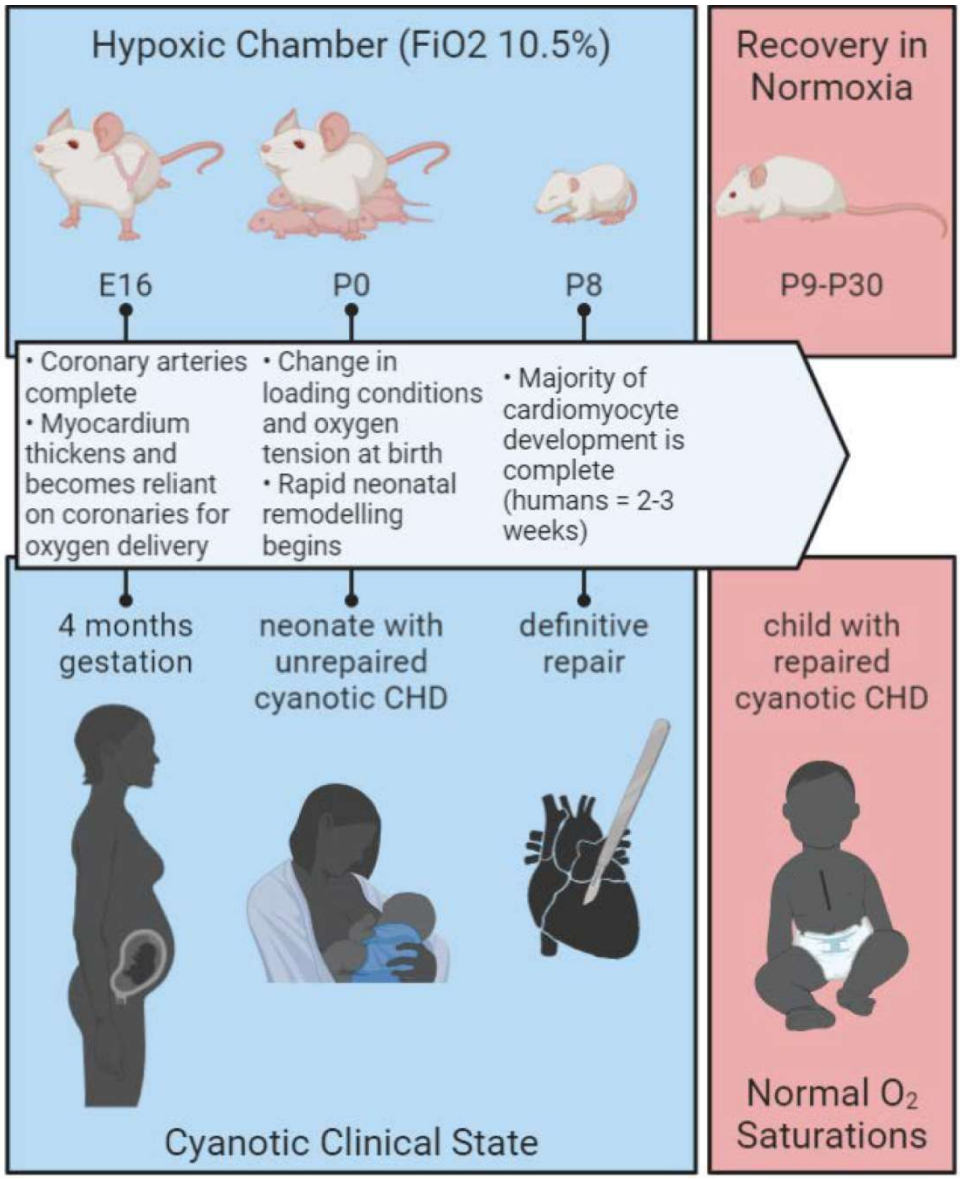

557

558 **Figure 1: Chronic Perinatal Hypoxia Mouse Model.** Pregnant CD1 mice were placed in
559 hypoxia starting on embryonic day (E)16, corresponding with rapid growth of the ventricular
560 myocardium and reliance on coronary arteries, similar to a 4 months gestation human fetus.
561 Hypoxic pups were born and reared in hypoxia until postnatal day (P)8 when the majority of
562 cardiomyocyte development is complete. Removal from the hypoxic chamber represents

563 definitive repair in human neonates with cyanotic CHD. Mice recovered in normoxia until further
564 testing at P30, representing a child with repaired cyanotic CHD and corresponding
565 normalization in oxygen saturations. FiO2, fractional inspired oxygen concentration. Image
566 created with Biorender.com.

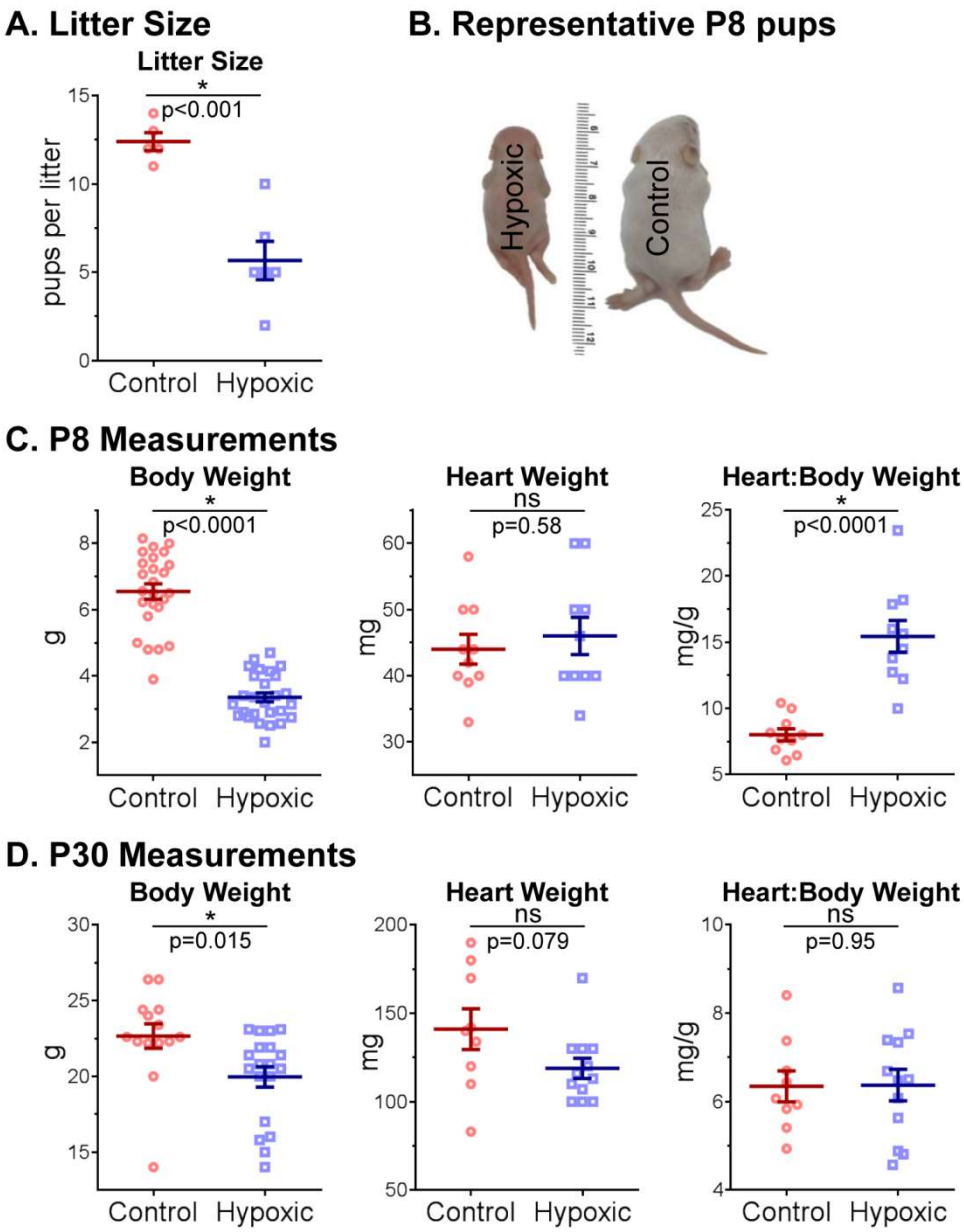

Figure 2: Litter Size and Body Measurements. A: Hypoxia reduced mean litter size. **B, C**: At P8, hypoxic animals were markedly smaller than control; however, heart weight was preserved, and thus heart-to-body-weight ratio was higher in hypoxic animals. **D:** By P30, hypoxic animals underwent catch-up growth such that they were only slightly smaller than control; heart weight trended toward slightly lower in hypoxic animals, and heart-to-body weight ratios were equivalent between groups. All data presented as mean ± SEM. *p<0.05, ns=not significant.

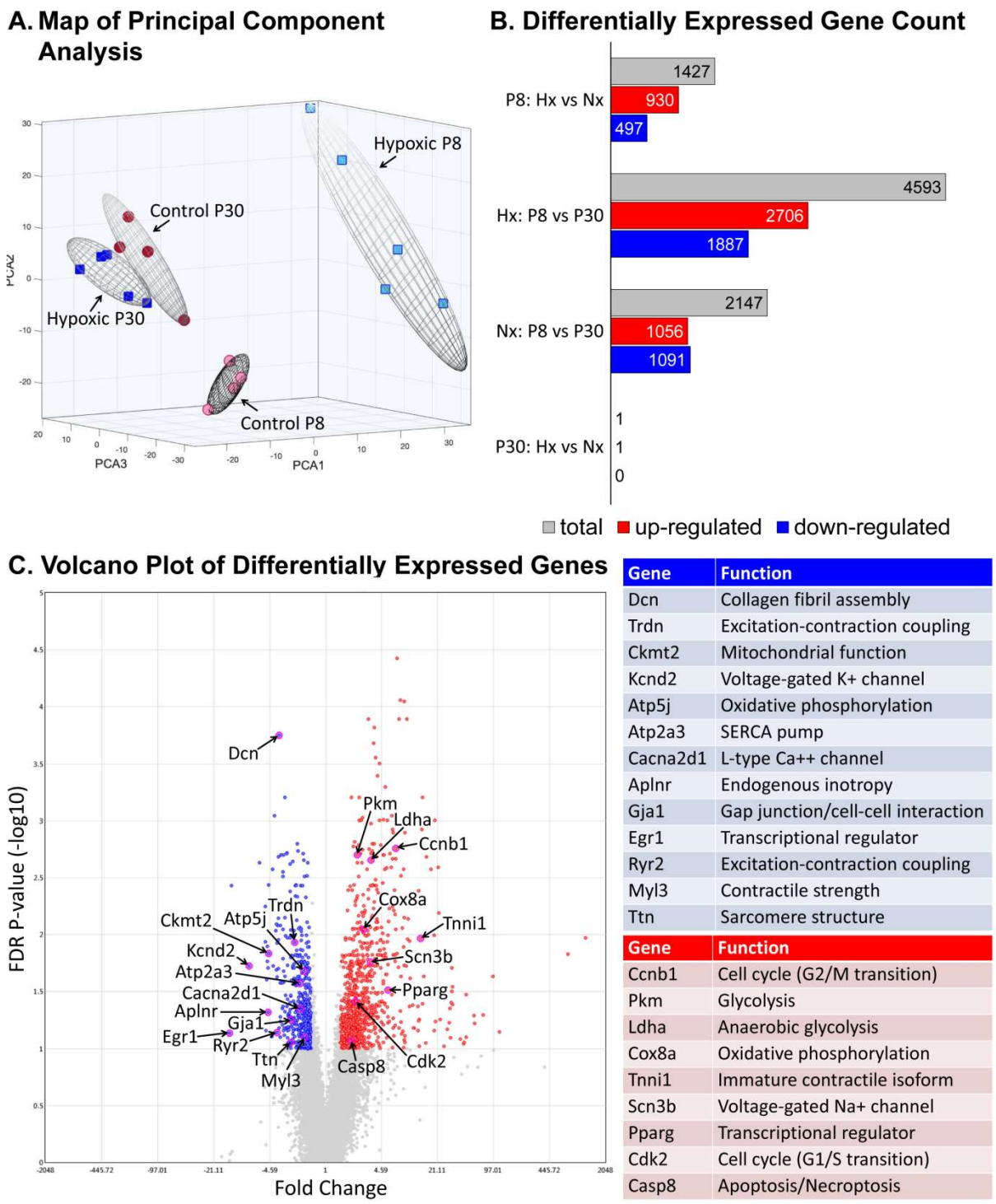

Gene	Function
Dcn	Collagen fibril assembly
Trdn	Excitation-contraction coupling
Ckmt2	Mitochondrial function
Kcnd2	Voltage-gated K+ channel
Atp5j	Oxidative phosphorylation
Atp2a3	SERCA pump
Cacna2d1	L-type Ca++ channel
Aplnr	Endogenous inotropy
Gja1	Gap junction/cell-cell interaction
Egr1	Transcriptional regulator
Ryr2	Excitation-contraction coupling
Myl3	Contractile strength
Ttn	Sarcomere structure

Gene	Function
Ccnb1	Cell cycle (G2/M transition)
Pkm	Glycolysis
Ldha	Anaerobic glycolysis
Cox8a	Oxidative phosphorylation
Tnni1	Immature contractile isoform
Scn3b	Voltage-gated Na+ channel
Pparg	Transcriptional regulator
Cdk2	Cell cycle (G1/S transition)
Casp8	Apoptosis/Necroptosis

Figure 3: Global Gene Expression. A: Principal component analysis demonstrated that experimental groups were well separated by their mRNA expression profiles at P8, but this separation was negligible in P30 samples. **B:** Using a 1.5-fold expression cut-off with 0.1 false-

578 discovery rate, a total of 1427 mRNAs were differentially expressed between hypoxic (Hx) and
579 normoxic control (Nx) hearts at P8, with near resolution of differences by P30. **C:** Specific genes
580 important to cardiovascular functioning and development are highlighted in a volcano plot of all
581 differentially expressed genes between groups at P8.

A. Gene Ontologies

Key Downregulated GOs	p	FDR q	Enrichment
Extracellular matrix structural constituent	5.42E-6	2.42E-3	5.08
Ion channel binding	2.52E-4	3.34E-2	2.90
Key Upregulated GOs	**p**	**FDR q**	**Enrichment**
Glycolytic process	3.66E-9	6.01E-6	19.00
Hypoxia-inducible factor-1alpha signaling pathway	1.70E-5	1.86E-3	47.65
Mitotic cell cycle process	1.63E-6	2.72E-4	2.11
Cell maturation	7.43E-4	3.4E-2	2.77

B. Gene Ontology Heat Maps

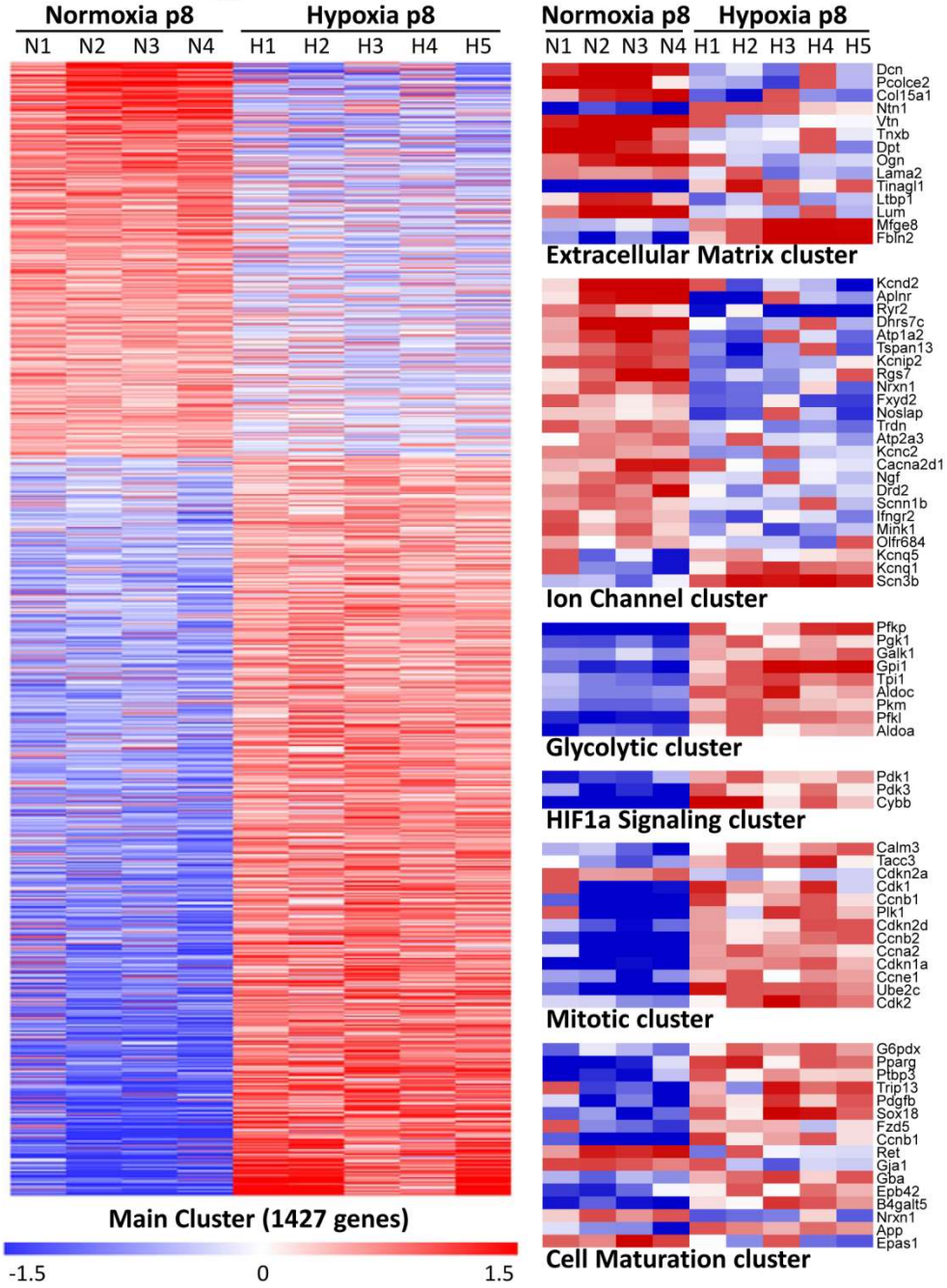

582

583 **Figure 4: Gene Ontologies. A:** Highlighted gene ontologies (GOs) important to cardiac
584 development and functioning that were different between groups at P8. **B:** Heat maps of the
585 main cluster of differentially expressed genes, as well as selected gene ontologies demonstrate
586 differential expression at P8 between groups. Each gene is median-centered, with data
587 displayed as fold-change.

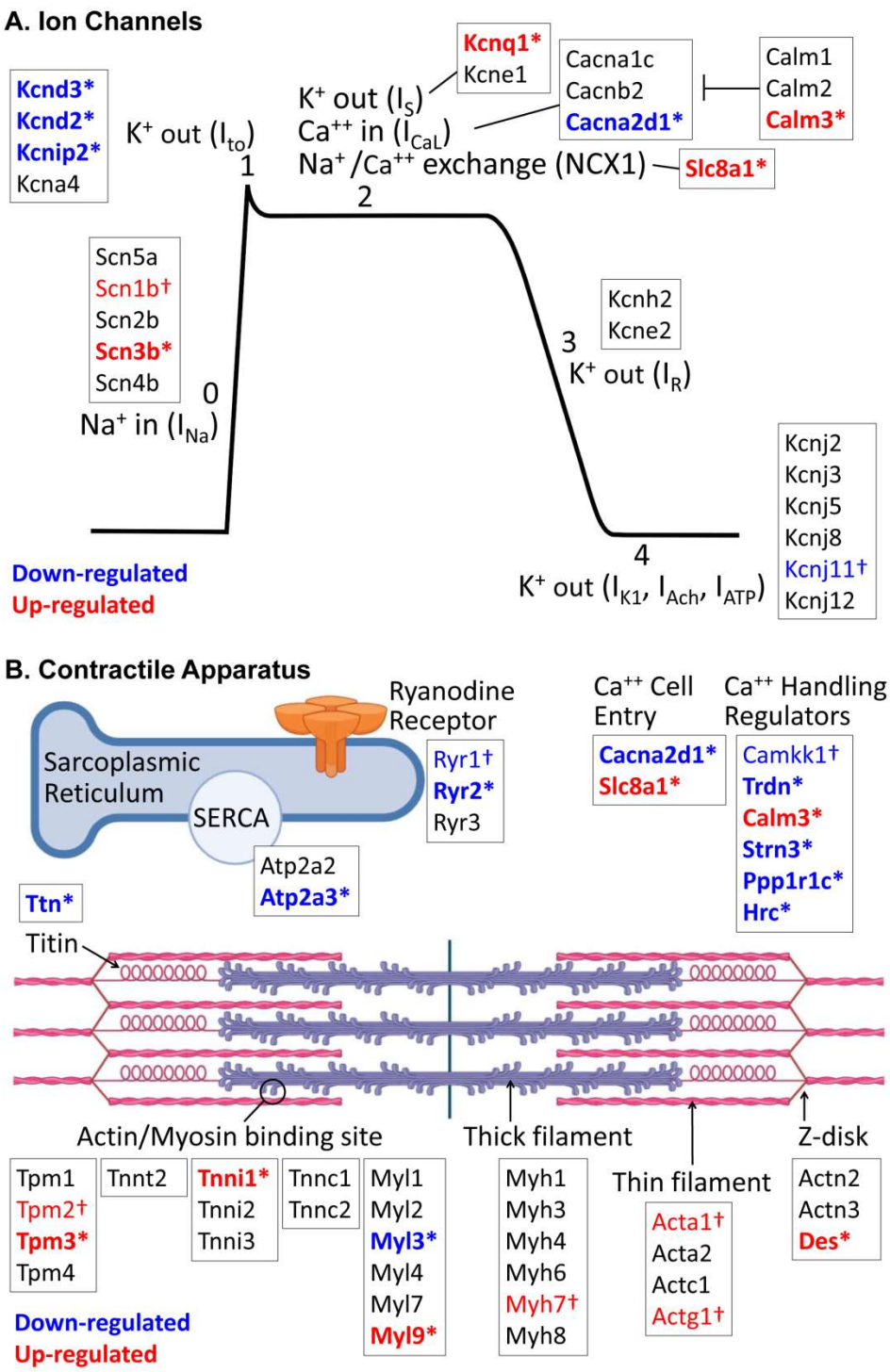

588

589 **Figure 5: Genes Affecting Ion Channels and the Contractile Apparatus. A:** At P8, hypoxia

590 affected genes involved with most phases of the cardiac action potential. **B:** Hypoxia affected

591 multiple genes important to the contractile apparatus, including both the sarcomere and calcium

592 handling machinery, at P8. *$p \leq 0.05$ and FDR $q \leq 0.1$ and †$p \leq 0.05$ and FDR $q > 0.1$. Image

593 created with Biorender.com.

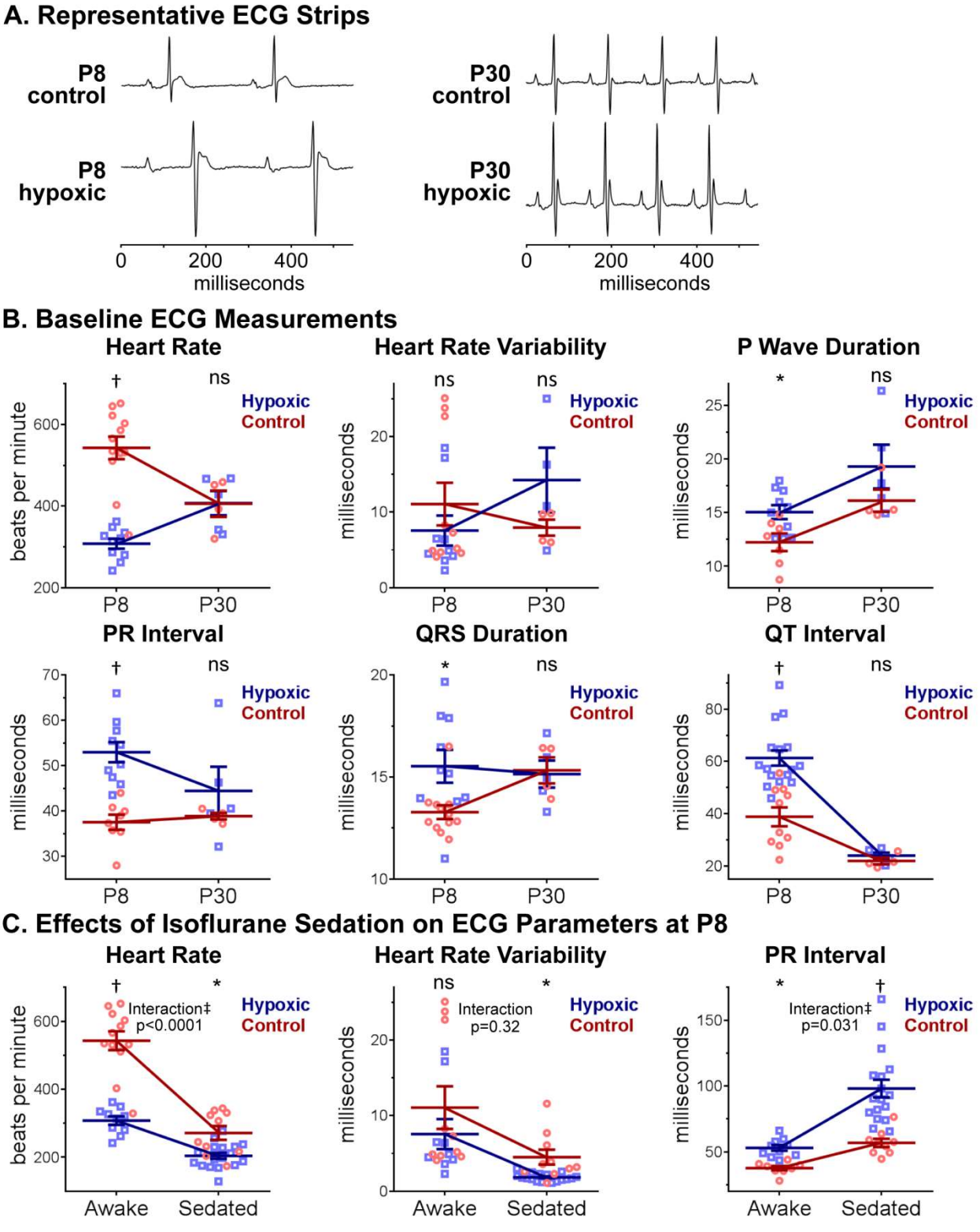

Figure 6: In-Vivo Electrocardiogram Measurements. A,B: Hypoxic P8 animals had lower heart rates compared to control, and hypoxia prolonged all ECG intervals measured, consistent

597 with slowed conduction speed. At P30, all ECG measurements had normalized. **C:** At P8,
598 isoflurane sedation caused more PR prolongation in hypoxic animals than control. Data
599 expressed as mean ± SEM. *$p<0.05$ hypoxic versus control. †$p<0.0001$ hypoxic versus control.
600 ‡$p<0.05$ for two-way ANOVA interaction between sedation and group. ns=not significant.

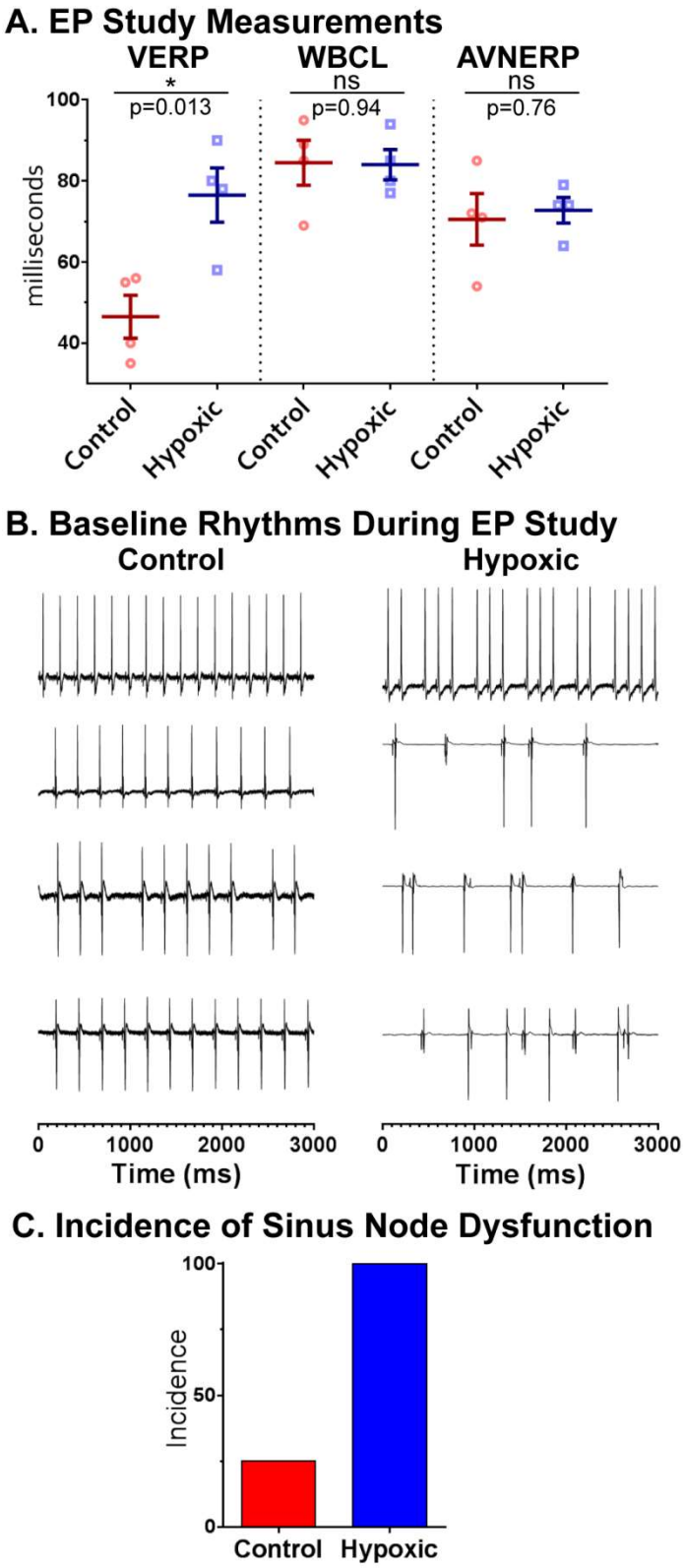

601

602 **Figure 7: Ex-Vivo Electrophysiology Study. A:** VERP was prolonged at P30 in animals

603 exposed to hypoxia. There was no difference for WBCL or AVNERP. **B:** Baseline rhythm during
604 electrophysiology studies is displayed for each animal. **B, C:** 100% of hypoxic and 25% of
605 control animals had sinus node dysfunction during the study. All data expressed as mean ±
606 SEM. VERP, ventricular effective refractory period. WBCL, Wenckebach cycle length. AVNERP,
607 atrioventricular nodal effective refractory period. *$p<0.05$. ns=not significant.

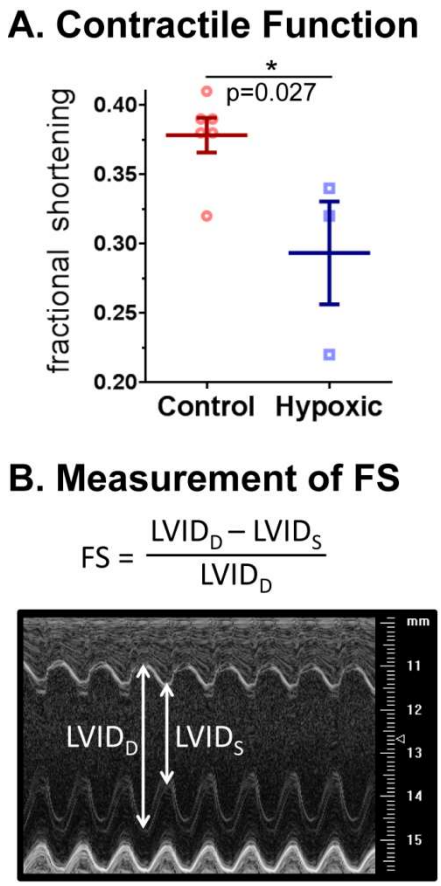

Figure 8: Contractile Function. A: Hypoxic animals had decreased contractile function compared to control, as measured by fractional shortening (FS). **B:** Measurements of the left ventricular internal diameter in systole ($LVID_S$) and diastole ($LVID_D$) were taken in M-Mode at the level of the papillary muscles from a parasternal short axis view. VevoSonics 770 with 30MHz high frequency ultrasound probe. Data expressed as mean ± SEM. *$p<0.05$.